Experimental evidence for moleculelike absorption and emission of porous silicon using far-field and near-field optical spectroscopy

Patrick J. Moyer* and Todd L. Cloninger
Department of Physics, The University of North Carolina at Charlotte, Charlotte, North Carolina 28223

James L. Gole
School of Physics, Georgia Institute of Technology, Atlanta, Georgia 30332-0430

Lawrence A. Bottomley
School of Chemistry and Biochemistry, Georgia Institute of Technology, Atlanta, Georgia 30332-0400
(Received 11 August 1998)

Far-field photoluminescence (PL) and near-field scanning optical microscopy (NSOM) have been used to provide insight into both the light emission and light absorption mechanisms of porous silicon (PS). Experiments were performed in air and in mercaptoethanol on two types of surface-prepared porous silicon samples. Dynamic studies on a time scale of the order of several minutes suggest that the surface state of the porous silicon is the principal determinant of the PL emission spectrum and the PL efficiency. From the results of experiments performed in various chemical environments, we infer that the PL emission may comprise multiple molecular spectral transitions. Further, variations in the nature of the PL as a function of excitation energy can be explained on the basis of the absorption of moleculelike species on the PS surface but not by the nature of absorption by nanocrystalline quantum structures. Finally, high-spatial-resolution NSOM spectroscopy is employed to determine that the spectral nature of the PL is spatially homogeneous down to a scale approaching 40 nm. Primarily, our experiments suggest that surface complexes are principally involved in the light emission from PS. Second, we also provide evidence that surface complexes, and not quantum confinement, may be responsible for the absorption of the incident excitation radiation. [S0163-1829(99)07727-9]

I. INTRODUCTION

The relatively large quantum efficiency of electroluminescent and photoluminescent processes from silicon samples which are appropriately electrochemically etched has drawn significant attention to porous silicon and the physics and chemistry determining its behavior.[1] There is controversy regarding the manner in which the porous structure forms, and the associated mechanism of the luminescence. The most widely considered models center around the assumption that quantum-size effects dominate the electronic energy structure of the small crystalline silicon features which are produced in the etching process. One model assumes that the photoluminescence (PL) results, following the optical pumping of electrons to an excited-state quantum level within a crystallite, by the radiative recombination of the electron-hole pairs within the crystallite.[1,2] A second model assumes that the photon is absorbed within individual crystallites, and produces an electron-hole pair which recombines externally from the crystallite within a recombination center or other type of trap.[3] Of course, these descriptions are quite general within the context of the two models.

In this paper, data are presented which are best explained with a third model:[4] one which is independent of the electronic structure of the nanocrystallites. Based upon the results which we outline, we suggest that the absorption of incident photons may take place within molecular complexes bound to the porous silicon surface (throughout the entire porous region). The emitted photons collected during the PL experiments would appear to result from the fluorescence of these excited surface fluorophores.

The experimental data presented and discussed in this paper involve far-field and near-field photoluminescence at two different excitation energies and under a variety of environmental conditions. The purpose of the near-field experiments is to determine the spectral nature of the PL emission on a scale of tens of nanometers. In near-field scanning optical microscopy (NSOM),[5] a subwavelength aperture (roughly 40 nm in diameter for the experiments performed here) is placed near to the sample using a force feedback method similar to that of atomic force microscopy. Thus, surface topography is mapped in addition to the PL with an excitation spot size 40 nm in diameter. This serves the purpose of probing a very small volume of the sample.

II. EXPERIMENT

A. Sample preparation

Two samples were studied via the experiments discussed in this paper. Sample A was fabricated in an electrochemical cell constructed from high-density polyethylene. The working electrode was attached to the back of a *p*-type silicon wafer (100), and the counterelectrode corresponded to a platinum foil placed in solution. The cell was sealed to the front of the wafer using a clamp such that a 1-cm^2 section of the wafer made contact with the solution. A magnetic stir bar was used to prevent the build up of hydrogen at the surface of the silicon. Current was supplied to perform the electrochemical etch using an EG&G Princeton Applied Research Potentiostat/Galvanostat (Model 273). The samples were

etched in a 1-M H_2O, 1-M HF, 0.1-M tetrabutylammonium perchlorate in acetonitrile solution with a current density of 8 mA/cm^2 for 1 h.

The second sample, sample B, corresponds to a single-crystal Si(100), boron-doped wafer of resistivity 1 Ω cm (MEMC, Dallas, TX) that was etched in an aqueous HF solution. For these aqueous HF experiments (20% concentration in methanol), a 300 nm thin film of aluminum was sputtered onto the back side of the wafer. Ohmic contacts were made to the wafer by connecting a wire to the thin film of aluminum using conductive paint (Insulating Materials, Inc., Ekote #3030). The wire and aluminum film were then covered with a layer of black wax (Apiezon W), leaving only the front surface of the silicon exposed to the etching solution. Both the silicon wafer wire and platinum electrode connections passed through a teflon cap which was tightly fit to a cuvette containing the etch solution. The etch current applied during aqueous etching was approximately 10 mA/cm^2. Typical etch times were on the order of 10 min. After etching, sample B was treated with a 1-M HCL/H_2O solution of about 1 M for the purpose of PL stabilization.

B. Far-field photoluminescence

Laser sources used for the far-field experiments include a 488-nm air-cooled argon-ion laser (Omnichrome) and a 351-nm/364-nm water-cooled argon-ion laser (Coherent Enterprise). The lasers were coupled to a single-mode optical fiber, and ported to a far-field experimental setup. A single-mode fiber allows one to direct the beam readily around an optical table as well as providing spatial filtering. Upon exiting the fiber, the light is incident upon a dichroic beamsplitter which reflects virtually all of the light below 515 nm and passes most of the light above 515 nm. The laser light was focused onto the sample using a 10× microscope objective with a numerical aperture of 0.15, so that the maximum power density at the sample was roughly 10^3 W/cm^2. The same microscope objective is used in a backscattering geometry to collect the light from the sample. After the light passes through the same dichroic beamsplitter, it passes through a 488-nm holographic notch filter (Kaiser Optical) for the purpose of removing those excitation source photons which have managed to transmit through the dichroic beamsplitter. The remaining light, which is then dominated by the porous silicon photoluminescence, is coupled into a multimode fiber. This fiber ports the light to a 0.5 m single-grating spectrometer. The spectra are collected in parallel using a liquid-nitrogen-cooled charge-coupled device (Princeton Instruments). The spectral resolution for all of the spectra displayed in this report is at least 2.0 nm in every spectral region.

C. Near-field photoluminescence

The same laser sources were used for both the far-field and NSOM experiments. For the NSOM experiments, the light is coupled into the single-mode fiber which has, at its distal end, a subwavelength aperture (typically of order 40 nm). Using shear force feedback or vertical tip dithering (as is typically used for ac-mode atomic force microscopy), the subwavelength aperture is maintained in the near-field sample. The NSOM (modified TopoMetrix Aurora) is operated in the reflection-mode, which has, as its collection optics, a long working distance 20× microscope objective with a numerical aperture of 0.35. The collected light passes through the 488-nm holographic notch filter before it is coupled into a multimode fiber for porting to a spectrometer. From this point, the experiment duplicates that which was described in the far-field experimental section (Sec. II B).

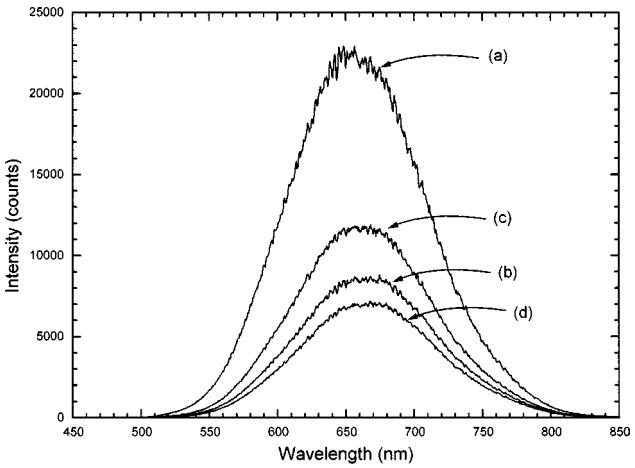

FIG. 1. Demonstration of light-induced quenching and recovery of sample A photoluminescence in air. These 5-s exposure spectra were acquired under 488-nm excitation. Spectrum (a) is acquired during the first 5 s and continuous illumination for two more minutes; spectrum (b) was acquired. The illumination beam was then blocked for 20 min allowing the sample PL to recover. The beam was then unblocked, and spectrum (c) was immediately acquired followed by spectrum (d) 2 min later.

III. RESULTS

Figure 1 displays the results of an experiment which examines the nature and decay of the far-field PL of sample A in air. The four PL emission spectra are each taken with 5-s CCD integration times under 488-nm excitation. The power density is roughly 10^3 W/cm^2. Each count on the vertical scale corresponds roughly to two photons. Spectrum (a) displays the counts as a function of wavelength for the first 5 s after illumination of a particular spot on the porous silicon (PS) surface. The sample was then continuously illuminated with the same power density for 2 min at that same sample position, at which time another spectrum was acquired [spectrum (b) in Fig. 1]. The laser was then blocked for 20 min before a third spectrum was acquired [spectrum (c)]. After two more minutes of continuous illumination, spectrum (d) was acquired. Note that the PL emission quantum efficiency decreases under continuous illumination, followed by a partial recovery when the excitation source is blocked. As we repeat this recycling-illumination procedure for several extended periods, we find that the samples continue to display a reversible partial recovery and similar decay under illumination. The ability to excite the PL emission continues to decrease in efficiency under continuous illumination.

One also notes that sample A displays some spectral variation in the PL emission with time. Figure 2 depicts the spectra (a) and (d) from Fig. 1 on a normalized scale. Here, spectrum (a) is 1× while spectrum (d) is approximately 3×. Along with the decay of the PL emission, as evident from

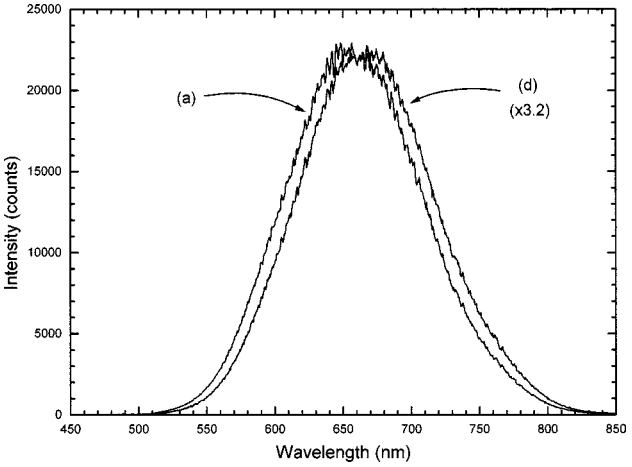

FIG. 2. Normalized rendering of the same spectra shown in Fig. 1. This normalized data presentation is intended to show the variations in spectral behavior during the light-induced decay and recovery process.

Fig. 1, one observes that the spectrum redshifts by about 25 nm (about 70 meV).

An NSOM PL emission spectrum was acquired for sample A and is depicted in Fig. 3, where it is compared with spectrum (d) from Fig. 2. In this figure the far-field spectrum [spectrum (d)] is shown at 1×, while the near field spectrum is shown at approximately 70×. The lateral spatial resolution of the NSOM experiment was determined, using a calibration sample, to be better than 40 nm. The calibration was performed in the reflection mode using a hexagonal-patterned aluminum island sample.[6] These islands are known to be less than 30 nm in diameter. The convolution of NSOM-measured features, in reflection mode, with feature size leads us to estimate the lateral resolution of our probe to be of order 40 nm. Thus, with an aperture output for this experiment of about 1 nW, the power density was approximately 10^2 W/cm^2. The CCD integration time is 30 s for the near-field spectrum.

It is significant that the near-field spectrum is qualitatively the same as the far-field spectrum, indicating the lack of spatial inhomogeneities down to a scale of about 40 nm. Photoluminescence images of the same sample indicate image contrast well over 50% of maximum intensity with a spatial resolution of less than 100 nm. This indicates that the nature of light spreading in the axial direction does not contribute significantly to a decrease of the spatial resolution of our spectroscopic measurement. This is not surprising considering the porous nature of the material, and the fact that isotropic scattering, as a function of depth into the material, will decrease the amount of light reaching the detector. Hence typical absorption constants for Si cannot be used to estimate the probed volume in the axial direction. Numerous NSOM spectra were taken across a region of $15\times15\,\mu$m^2, all of which duplicated the NSOM spectrum shown in Fig. 3. The only spectral variations were found to occur near the edge of the porous region, indicating a lack of homogeneity in the PS fabrication conditions at the boundary (most notably, current density and effects on the boundary layer due to diffusion).

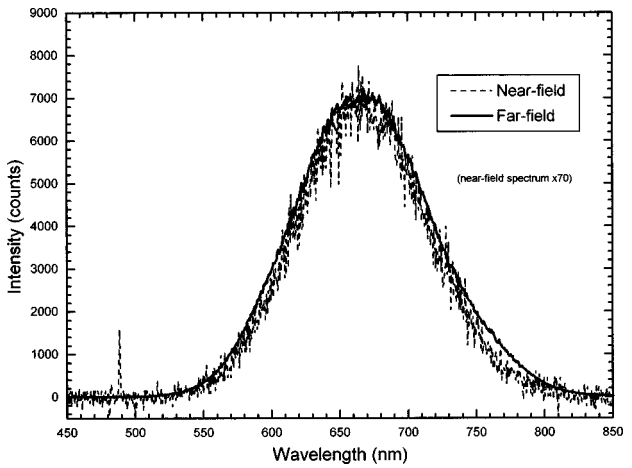

FIG. 3. NSOM PL spectrum of sample A compared with far-field spectrum of the same sample [spectrum (d) from Fig. 2].

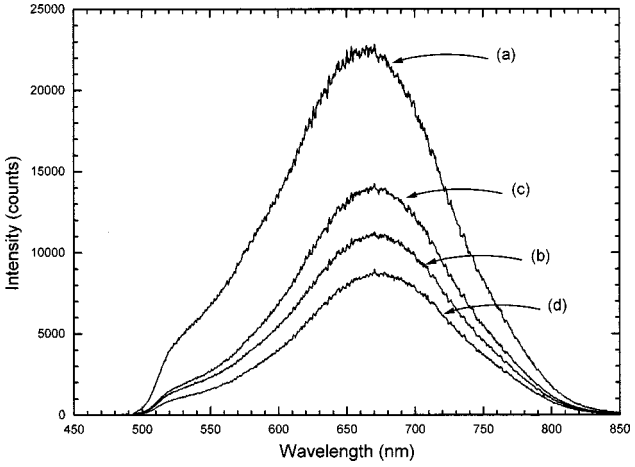

FIG. 4. Demonstration of light-induced quenching and recovery of sample B photoluminescence in air. These 5-s exposure spectra were acquired under 488-nm excitation. Spectrum (a) is acquired during the first 5 s and continuous illumination for two more minutes; spectrum (b) was acquired. The illumination beam was then blocked for 20 min, allowing the sample PL to recover. The beam was then unblocked and spectrum (c) was immediately acquired followed by spectrum (d) 2 min later.

Figure 4 depicts PL emission spectra for sample B acquired in air under the same conditions as those shown in Fig. 1. Spectrum (a) was again the first acquired spectrum, followed by spectrum (b) taken 2 min later following continuous illumination. The *cw* beam was then blocked for 20 min, after which spectra (c) and (d) were acquired, with (d) being acquired after 2 min of continuous illumination. Figure 5 depicts spectra (a) and (d) from Fig. 4, normalized so that spectral variations can be evaluated. Figures 4 and 5 demonstrate the onset of a distinct spectral feature, in particular a higher-energy peak at about 520 nm. This ''green'' peak is considerably more sensitive to decay under 488-nm illumination as it appears to decrease much more rapidly than the dominant longer wavelength feature.

The 488-nm excitation laser was replaced by a 364-nm excitation laser, and further PL emission spectra were acquired for sample B. These data are shown in Fig. 6. The total laser power incident on the sample was approximately 0.15 μW, resulting in a power density of approximately 1 W/cm^2. Note that this is three orders of magnitude lower

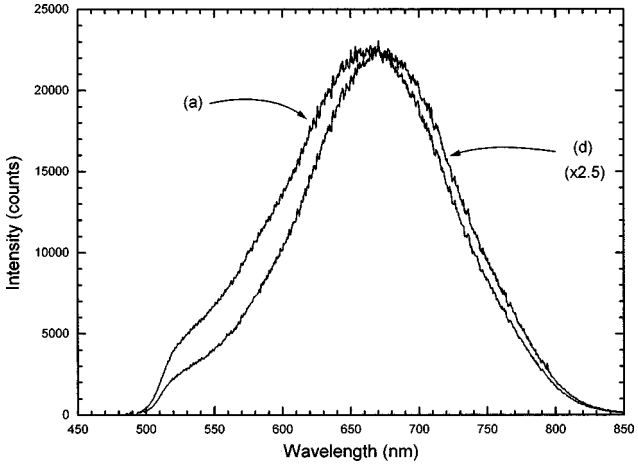

FIG. 5. Normalized rendering of the same spectra as shown in Fig. 4. This normalized data presentation is intended to show the variations in spectral behavior during the light-induced decay and recovery process.

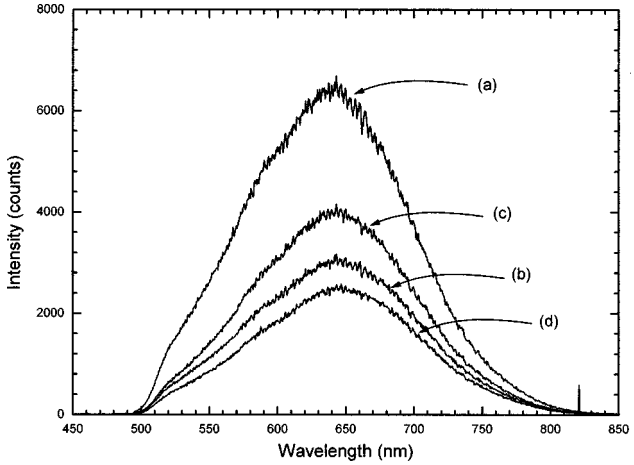

FIG. 7. Demonstration of light-induced quenching and recovery of porous silicon photoluminescence in mercaptoethanol. These 5-s exposure spectra were acquired under 488-nm excitation. Spectrum (a) is acquired during the first 5 s and continuous illumination for two more minutes; spectrum (b) was acquired. The illumination beam was then blocked for 20 min, allowing the sample PL to recover. The beam was then unblocked and spectrum (c) was immediately acquired followed by spectrum (d) 2 min later.

than the power density incident on the sample when using the 488-nm argon-ion line for PL excitation. Spectrum (a) was acquired immediately after exposing the sample, while spectrum (b) was acquired following 2 min of continuous illumination. Recovery data are not shown here for the sake of simplicity; however, they were acquired and show the same partial recovery effects suggested in Figs. 1 and 4. We note the complete absence of the green peak when the PS sample is excited by 364-nm laser radiation (Fig. 6). In addition, the dominant spectral emission maximum blueshifts by about 20 nm versus that for the same sample (sample B), where PL is excited with 488-nm radiation. Finally, if we assume that the PL excitation quantum efficiency is linear with excitation intensity up to at least 10^3 W/cm^2, then the extrapolated peak count for 5 s at 364-nm excitation would be roughly 300 000 counts (accounting also for the change in energy per photon for 488 nm vs 364 nm). This indicates an increase of PL excitation quantum efficiency at 364 nm of roughly a factor of 15 over that for 488-nm excitation. This observation is quite consistent with known PL excitation data.[7,8]

The dynamics of the PL emission spectrum observed for sample B was also probed while the sample was immersed in a mercaptoethanol environment. Figure 7 depicts the alteration of the spectral intensity distribution which results from this immersion. Normalized intensity data from the same experiment are shown in Fig. 8. These data were acquired using 488-nm excitation. In this set of experiments, the 520-nm green peak is clearly present as well as the possible indication of a feature resulting from an apparent transition in the range near 590 nm. As a result of the increase (or onset) in spectral intensity at area 590 nm, the peak of the PL transmission maximum appears to have blue-shifted by roughly 20 nm from 660 to 640 nm.

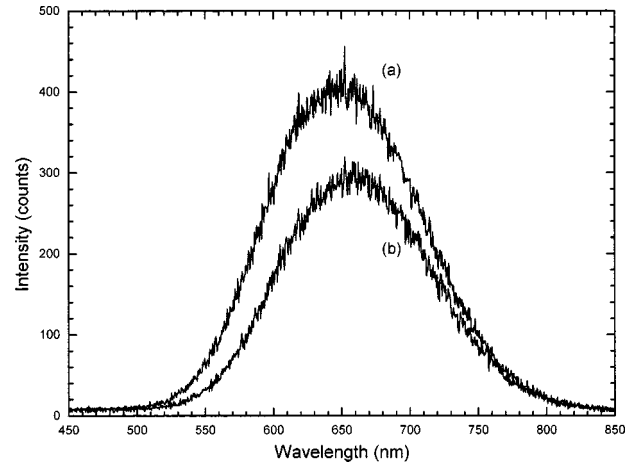

FIG. 6. Photoluminescence of sample B in air under 364-nm excitation. Of particular interest is the disappearance of the 520-nm shoulder which was previously present when the PL was excited with 488-nm radiation.

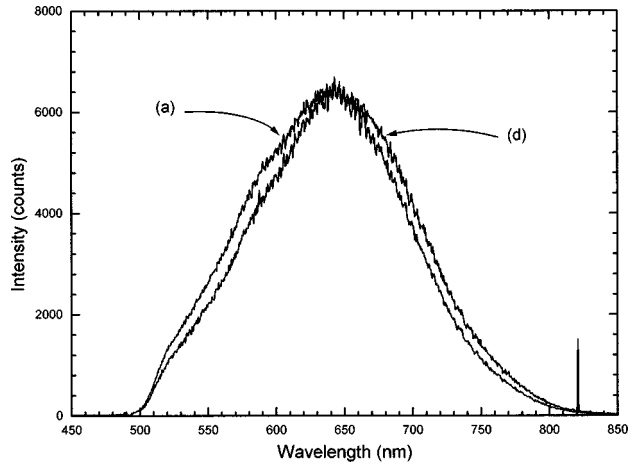

FIG. 8. Normalized rendering of the same spectra as shown in Fig. 7. This normalized data presentation is intended to show the variations in spectral behavior during the light-induced decay and recovery process.

IV. DISCUSSION OF EXPERIMENTAL RESULTS

Significant observations made in the present study include: (1) the PL decay dynamics under illumination and the subsequent recovery of the PL in darkness; (2) the photoluminescence from the green emission feature at 520 nm and its dependence on the laser excitation wavelength; (3) the influence of the radical scavenger mercaptoethanol on the PL emission spectrum; and (4) the close agreement of far-field and NSOM PL emission spectra. In the following paragraphs, each finding will be examined in the context of the existing models of PS emission.

Figures 1, 4, and 7 provide compelling evidence that the photobleaching of the PS emission is at least partially reversible. The observation of PL decay under illumination and its subsequent partial recovery after 20 min in darkness at ambient temperature (Figs. 1, 4, and 7) clearly indicates that the decrease in PL quantum efficiency cannot be the result of the annealing of nanocrystalline structures since the nanocrystallite annealing would be an irreversible process. The observed PL decay and restoration, which has been reversibly recycled for periods of far greater extent than indicated in the figures, is consistent with a surface localized process, i.e., either through the photoexcitation or photoionization of surface complexes or by saturation of radiative recombination sites. We do not conclude from this result that nanocrystallites are not present. In lieu of the PL recovery (albeit partial in some cases), we do, however, conclude that annealling nanocrystallites cannot be a valid explanation of the decrease in PL efficiency during illumination. Thus surface states or surface complexes are, at the very least, heavily involved in the PL emission process.

It is worth noting that this conclusion is well supported by the evaluation of the effects of hydrostatic pressure dependence, at hydrostatic pressures on the PL from porous silicon by Cheong *et al.*[9] The anomalous PL pressure dependence at hydrostatic pressures up to 60 kbar, which these authors observed under a helium or standard 4:1 methanol:ethanol mixture (1) is not exclusively an intrinsic property associated with PS, and (2) is consistent with a process involving states at or near the surface of the PS. The exact nature of the incident photon absorption mechanism cannot be elucidated by the present experimental results; however, based on supplementary information it is possible to consider what the surface states or surface complexes might be.

It is known that anhydrous HF etching to form a PS surface will create a SiH_x termination in the absence of any oxygen donors.[10,11,12] In contrast, the ready formation of the oxyhydrides has been noted for samples which have are prepared in an aqueous etch environment.[4f,13] While some reported photoelectron spectra[14] have been interpreted to suggest that there is no oxygen on a freshly prepared PS surface, this interpretation must be questioned as the observed photoemission spectrum for the Si $2p$ core level shows a substantial tail to high energy. This, of course, is considered to be an excellent indication of suboxide formation. In fact, infrared spectra on freshly formed and air oxidized samples[15] suggest a surface oxide formation which may be interpreted to result from oxyhydride formation.[16] Recently, the stabilizing effect of water on the PS luminescence and its potential influence on the mechanism for the HF etching of a PS surface has been carefully considered and evaluated.[16] Here again, the oxyhydrides are implicated as important surface constituents.[17] Finally, similar behaviors are noted for silicon nanoparticles[18] and colloidal suspensions,[19(a),19(b)] again suggesting the role of oxyhydrides in the etch process.

We have observed that the 520-nm shoulder present in Fig. 4 (under 488-nm excitation) completely vanishes under 364-nm excitation (Fig. 6). The PS luminescence is characterized by the transformation of an initial green emission feature to a final ''orange-red'' emission feature.[8] The current observation that the intensity of emission at 520 nm i.e., the green emission feature) depends on laser excitation wavelength provides insight into the transformation process, and enables further discrimination of the proposed models for PS luminescence.[8] We suggest (1) that the green emission feature emanates from a surface-confined precursor state that is chemically transformed to a final orange-red emitter, and (2) that the 488-nm laser excitation line lies within the absorption profile of this precursor state whereas the 364-nm laser excitation line does not. In contrast to our observation, the quantum confinement model predicts that the probability of photon absorption for quantum-confined states nominally increases as the photon energy increases provided the energy is larger than the initial transition edge. The intensity of the feature at 520 nm is therefore expected to increase as the laser excitation wavelength is shifted from 488 to 364 nm. Figures 4 and 6 clearly demonstrate that this is not the case. We also suggest that the surface-confined precursor state, after absorbing a 488-nm photon, can more readily undergo oxidative transformation (see the following).

The temporal nature and spectral characteristics of the PL emission strongly depend upon the local environment at the PS-air or PS-solution interface. For example, when PS is photoexcited in air, the emission feature at 520 nm decays at a rate 50% faster than that of other features in the spectrum. In contrast, when PS is photoexcited in a solution containing mercaptoethanol, the rate of decay of the feature at 520 nm is the same as that of other features in the spectrum. Thus mercaptoethanol, a known radical scavenger, is stabilizing the source of the 520-nm emission feature relative to the source of the orange-red emission feature.[8]

The green and orange-red PL emissions characteristic of PS can be excited with a variety of uv light sources and observed during and directly following the *in situ* (in solution) etching of a PS surface in 20% HF in MeOH solution or 20% HF in H_2O solutions.[8] Experimental observations of the time-dependent behavior of this *in situ* PL can be combined with quantum chemical modeling of the low-lying electronic states of the silanone-based silicon oxyhydrides[20,21] to suggest that the initially observed and relatively long-lived green PL, its subsequent transformation to a final orange-red emission, and its stabilization in an ethylene glycol solution are to be associated with oxyhydride electronic transitions and the chemical transformation of surface-bound oxyhydrides.[4]

A recently proposed model to explain the outlined PL transformation is best outlined considering the data given in Tables I and II. Here we summarize SiO bond lengths and electronic energies obtained from detailed molecular electronic structure calculations (MP2-DZP level of description,[20–22] where MP2 represents the Moller-Plesset

TABLE I. Si=0 bond lengths (Å) for silanones at the MP2/DZP level of description.

Molecule	r(SiO) singlet	r(SiO) triplet	Δr(SiO)
Si(O)H2	1.545	1.700[a]	0.155
$Si(O)(SiH_3)_2$	1.560	1.681	0.121
$Si(O)H(SiH)_3$	1.553	1.695	0.142
Si(O)H(OH)[b]	1.537	1.709	0.172
$Si(O)SiH_3(OH)$	1.543	1.712	0.169
$Si(O)H(OSiH_3)$	1.537	1.708	0.171
$Si(O)SiH_3(OSiH_3)$	1.543	1.712	0.169
$Si(O)(OH)_2$	1.536	1.709	0.173
$Si(O)(OSiH_3)_2$	1.537	1.708	0.171

[a]Bond length for the excited singlet is 1.705 Å.

[b]Bond lengths for HO-Si-OH silylene are 1.670 Å for the ground-state singlet and 1.680 Å for the excited triplet.

optimization and DZP represents the polarized double-ζ basis set) for the ground-state singlets and lowest-lying excited-state triplets of those silanone-based oxyhydride compounds which appear to closely mimic the absorption and emission characteristics observed for a PS surface.[10,11] Table I demonstrates that a significant change accompanies the silanone transitions to the excited triplet state. This state can be identified with the triplet exciton characterized by Stutzmann and co-workers.[4(c)–4(e)] The transition produces a significant lengthening of the SiO bond which is not observed for the silylene isomers.[21]

The data in Table II are noteworthy in that the locations of the unsaturated silanone-based silicon-oxyhydride triplet states and the known peak wavelength of the porous silicon PL excitation spectrum (PLE) (area 350 nm)[7] bear a close resemblance. The large change in the SiO bond lengths associated with the silanones (indicated in Table I) in turn, produces a large shift in their excited-state potentials relative to the ground state. The location of the ground- and excited-state potentials can promote optical pumping high up the excited-state potential. Thus, in absorption, we anticipate a shift to higher energies than the adiabatic energy separation corresponding to the peak in the PLE excitation spectrum (area 350 nm, and a significant redshift in the observed PL emission range (area 580–800 nm).[20,21] The data in Table I also indicate that when an -OH or $-OSiH_3$ group is bound to the silicon-oxygen bond, the change $\Delta[r(\mathrm{SiO})]$ in transition is consistently of order 0.17 Å. Further, the adiabatic energy increment is consistently of order 3.05 eV. By comparison, for $Si(O)H_2$, $Si(O)H(SiH_3)$, and $Si(O)(SiH_5)_2$, the change in bond length is notably smaller, decreasing from 0.155 to 0.121 Å. This suggests that the peak of the PLE excitation spectra and the PL emission spectra associated with these silanones will not differ to the extent associated with the silicon oxyhydrides containing an -OH or -O*R* group. We thus anticipate a considerably smaller redshift in the PL emission spectrum.

TABLE II. Ground-state singlet-ecited-state energy separation for silaones and silylenes.

Molecule	$\delta E(S\text{-}T)$ (kcal/mol)	$\Delta E(S\text{-}T)$ (eV)	$\sim\lambda_{\mathrm{adiabatic}}$ (nm)
Si(O)H2	60.1	2.60	475
$Si(O)(SiH_3)_2$	53.9	2.34	530
$Si(O)H(SiH_3)$	57.3	2.48	499
Si(O)H(OH)	70.9	3.07	403
$Si(O)SiH_3(OH)$	71.3	3.09	401
$Si(O)H(OSiH_3)$	70.4	3.05	406
$Si(O)SiH_3(OSiH_3)$	69.6	3.02	411
$Si(O)(OH)_2$	71.1	3.08	402
$Si(O)(OSiH_3)_2$	67.1	2.91	426
HSiOH	38.4	1.66	744
HOSiOH	64.2	2.78	445
SiH_3OSiH_3	67.4	2.92	425

The adiabatic transition energies given in Table II also suggest that the excited triplet states associated with precursors of the form $Si(O)H_2$, $Si(O)H(SiH_3)$, and $Si(O)(SiH_3)_2$ should be readily accessed by the argon ion laser line at 488 nm (514.5 nm), whereas the subsequently oxidized silanones containing an -OH or -O*R* group are best pumped at 350 nm, the peak in the PS absorption most commonly observed. In other words, we suggest that the source of the green 520-nm emission feature corresponds to a precursor -H or -*R* group (to SiO) bound oxyhydride emitter which can best be accessed by the strong argon-ion laser line at 488 nm which is blueshifted relative to its adiabatic transition energy. Further, if the 520-nm green emission feature is associated with a transition involving a long-lived excited triplet state, we suggest that the observed decay of the 520-nm fluorescence feature in air results from an enhanced excited state oxidation, converting the initial oxyhydride to the -OH or -O*R* bound fluorophor which subsequently emits at much longer wavelength. Finally, we note that the stabilization of the 520-nm emission in mercaptoethanol, $HSCH_2CH_2OH$, solution is quite consistent with the observed stabilization of this green emitter in an analog ethylene glycol $HOCH_2CH_2OH$, solution.[8] We thus suggest that the behavior of the 520 emission feature in mercaptoethanol and as a function of laser pump wavelength is consistent with the optical pumping of a surface bound source of the form O═Si-*R* where *R*═H, SiH_3.

We have presented a model to explain the ''green'' and ''orange-red'' PL features based on formation of surface bound silanone-based silicon oxyhydrides. We also note that an extension of this model which includes the further efficient oxidation of the pumped long-lived silanone triplet states to form SiO_2 constituencies on the PS surface can explain the irreversible reduction in the PL intensity with laser pumping. When oxidation to SiO_2 occurs, the PS surface site is no longer photoluminescent. We thus suggest that the creation of both the silanones and SiO_2 can account for the nature of the cycling which we observe in the current experiments. Henglein and co-workers.[19(a),19(b)] studied luminescence colloidal silicon particles prepared from HF-eteched oxide-coated crystalline silicon formed in the combustion of silane. They find that the orange-red PL can be activated by the aqueous HF etching of the silicon particles suspended in a 1:1 cyclohexane-propanol-2 solution in the presence of air. The required presence of oxygen (under argon there is no luminescence) in these solution phase studies appears to indicate that the oxide layer created in the com-

bustion of silane does not promote luminescence. Rather, as Heinglein and co-workers noted, the development of the orange-red PL in nonpolar cyclohexane suggests that this original oxide layer must first be removed by HF. The silicon particles, with a nonpolar surface, are created in the cyclohexane phase. Here an equilibrium is established between their surface oxidation and reduction by O_2 and HF, respectively. Near pristine silicon colloidal particles are formed whose oxidation, *to a much lower level than the original oxide-coated particles*, produces luminescence. These authors suggest that the orange-red PL occurs when colloidal silicon particles carry only a limited component of oxidized centers, and that the protonation state of these centers strongly affects the luminescence. These results are also consistent with the outlined model and cycling behavior which we have observed.

Finally, we have obtained over 100 near-field emission spectra under identical conditions and with a spatial resolution of 40 nm as a single probe was repositioned across a PS sample domain of $15\times15\ \mu m^2$. All spectra were found to be identical within the 2-nm spectral resolution of our system. The close agreement of the near- and far-field emission spectra would appear to be inconsistent with models based on emission from nanocrystallites. In fact, it would seem that the crystallite size distribution across the PS sample could not be homogeneous on the scale of the NSOM probe such that spectral variations due to absorption, emission, or both would not be observed. From a quantitative basis, if we estimate the probed volume to be roughly $10^{-4}\ \mu m^3$, the size of the average nanocrystallite to be 5 nm, and a 75% porosity, then each spectrum averages roughly 100 nanocrystallites. With a spectral resolution of 2 nm and a total width of the spectra of nearly 200 nm, we would expect some variations in ensemble averaging with this type of spatial resolution if, in fact, nanocrystallites were responsible for the PL emission. However, it would not be surprising to monitor surface complexes with a homogeneous distribution on this length scale. Mason *et al.* also showed that the broad nature of the PL emission spectrum from PS is not a result of ensemble averaging from a large number of particles.[23] In their study, PS nanoparticles were isolated and spectrally analyzed with PL emission spectra showing widths well over 100 nm. Thus, despite the spectral shifts from particle to particle, the width of the individual spectral features indicate that (1) surface species play a primary role in the light emission mechanism, and (2) few particles would be necessary to ensemble average into the homogeneously broadened spectra that we observe. Thus we reference the work of Mason *et al.* in support of our conclusion that the energy structure of surface bound complexes must play a critical role in the light emission process.

V. SUMMARY

A consideration of all of the above-mentioned experimental results and surface modeling suggests that the observed far-field and NSOM PL emissions are strongly dependent on surface species. The data clearly suggest a strong dependence of the quantum efficiency and the nature of the observed emission on the PS surface and the chemistry which it undergoes.

To best explain the photoluminescence from PS, we have considered the fluorescence behavior of a number of individual molecule-like or defect states. Dependent upon the environment, the density and type of moleculelike fluorophors on the surface will change, as will their respective selection rules. Each of these species has its own spectral absorption, and subsequent emission based largely upon the nature of its functional groups and its local environment. The observed variations and qualitative behavior outlined here are quite consistent with a moleculelike absorption and emission. Furthermore, our observations do not appear to be explicable using the quantum confinement model.

ACKNOWLEDGMENTS

We thank Peter Lillihei and Lenward Seals for their help in sample preparation, as well as Dr. Sharka Prokes for insightful comments. P.J.M. would like to thank The University of North Carolina at Charlotte for support through startup funds and the Faculty Development Grant Program, as well as helpful discussions with Professor Jordan Poler. J.L.G. and L.A.B. acknowledge financial support from the Office of the President at Georgia Institute of Technology under the auspices of the Focused Research Program.

*Author to whom correspondence should be addressed. Electronic address: pjmoyer@email.uncc.edu

[1] For a comprehensive review, see A. G. Cullis, L. T. Canham, and P. D. J. Calcott, J. Appl. Phys. **83**, 909 (1997).

[2] See, for example, P. D. J. Calcott, K. J. Nash, L. T. Canham, M. J. Kane, and D. Brumhead, J. Phys.: Condens. Matter **5**, L91 (1993); J. Lumin. **57**, 257 (1993); K. J. Nash, P. D. J. Calcott, L. T. Canham, and R. J. Needs, Phys. Rev. B **51**, 17 698 (1995).

[3] F. Koch, V. Petrova-Koch, T. Muschik, A. Nikolov, and V. Gavrilenko, in *Microcrystalline Semiconductors: Materials Science & Devices*, edited by P. M. Fauchet, C. C. Tsai, L. T. Caham, I. Shimizu, and Y. Aoyagi, MRS Symposia Proceedings No. 283 (Materials Research Society, Pittsburgh, 1993), p. 197; F. Koch, V. Petrova-Koch, and T. Muschik, J. Lumin. **57**, 271 (1993); F. Koch, in *Silian-Based Optoelectronic Materials*, edited by M. A. Tischler, R. T. Collius, M. L. Thewalt, and G. Austreiten, MRS Symposia Proceedings No. 298 (Materials Research Society, Pittsburgh, 1993), p. 222. Y. H. Xie, W. L. Wilson, F. M. Ross, J. A. Mucha, E. A. Fitzgerald, J. M. Macauley, and T. D. Harris, J. Appl. Phys. **71**, 2403 (1992).

[4] (a) S. Prokes, O. J. Glembocki, V. M. Bermudez, R. Kaplan, L. E. Friedersdorf, and P. C. Shearson, Phys. Rev. B **45**, 13 788 (1992); (b) S. M. Prokes, J. Appl. Phys. **73**, 407 (1993); (c) H. D. Fuchs, M. Rosenbauer, M. S. Brandt, S. Ernst, S. Finkbeiner, M. Stutzmann, K. Syassen, J. Weber, H. J. Queisser, and M. Cardona, in *Microcrystalline Semiconductors: Materials Science & Devices* (Ref. 3), p. 203; (d) M. Stutzmann, M. S. Brandt, M. Rosenbauer, H. D. Fuchs, S. Finkbeiner, J. Weber, and P. Deak, J. Lumin. **57**, 321 (1993); (e) M. S. Brandt and M. S. Stutzmann, Solid State Commun. **93**, 473 (1995); (f) A. J. Steckl, J. Xu, H. C. Mogul, and S. M. Prokes, J. Electrochem. Soc. **142**, L69 (1995); (g) S. M. Prokes and O. J. Glembocki, Phys. Rev. B **49**, 2238 (1994); (h) S. M. Prokes, W. E. Carlos, and O. J. Glembocki, *ibid.* **50**, 17 093 (1994); (i) W. E. Carlos and S. M. Prokes,

J. Appl. Phys. **78**, 2129 (1995); (j) S. M. Prokes and W. E. Carlos, *ibid.* **78**, 2671 (1995).
[5] Michael A. Paesler and Patrick. J. Moyer, *Near-Field Optics: Theory, Instrumentation and Applications* (Wiley-Interscience, New York, 1996).
[6] For an example of such a sample, see Patrick J. Moyer and Stefan B. Kammer, Appl. Phys. Lett. **68**, 3380 (1996).
[7] See, for example, L. E. Brus, P. F. Szajowski, W. L. Wilson, T. D. Harris, S. Schuppler, and P. H. Citrin, J. Am. Chem. Soc. **117**, 2915 (1995).
[8] See, for example, J. L. Gole and D. A. Dixon, J. Phys. Chem. **103**, 33 (1998).
[9] H. M. Cheong, P. Wickboldt, D. Pang, J. H. Chen, and W. Paul, Phys. Rev. B **52**, R11 577 (1995).
[10] H. Gerischer, P. Allongue, and V. C. Kieling, Ber. Bunsenges. Phys. Chem. **97**, 753 (1993).
[11] E. K. Propst and P. A. Kohl, J. Chem. Soc. **141**, 1006 (1994).
[12] G. W. Trucks, K. Ragahavachari, G. S. Higashi, and Y. J. Chabal, Phys. Rev. Lett. **65**, 504 (1990).
[13] J. Yan, S. Shih, K. H. Jung, D. L. Kwong, M. Kovar, J. M. White, B. M. Gnade, and L. Magel, Appl. Phys. Lett. **64**, 1374 (1994).
[14] T. van Buren, T. Tiedje, J. R. Dahn, and B. M. Way, Appl. Phys. Lett. **63**, 2911 (1993).
[15] D. B. Mawhinney, J. A. Glass, Jr., and J. T. Yates, Jr., J. Phys. Chem. B **101**, 1202 (1997).
[16] J. L. Gole and D. A. Dixon, J. Phys. Chem. B **101**, 8096 (1997).
[17] F. P. Dudel and J. L. Gole, J. Appl. Phys. **82**, 802 (1997); J. L. Gole, F. P. Dudel, L. Seals, M. Reiger, P. Kohl, and L. A. Bottomley, J. Electrochem. Soc. **145**, 3284 (1998).
[18] J. L. Gole and D. A. Dixon, J. Appl. Phys. **83**, 5985 (1998).
[19] (a) A. Fojtik and A. Henglein, Chem. Phys. Lett. **221**, 363 (1994); (b) A. Fojtik, M. Giersig, and A. Henglein, Ber. Bunsenges. Phys. Chem. **97**, 1493 (1993).
[20] J. L. Gole, F. P. Dudel, D. R. Grantier, and D. A. Dixon, Phys. Rev. B **56**, 2137 (1997).
[21] See, for example, J. L. Gole and D. A. Dixon, Phys. Rev. B **57**, 12 002 (1998).
[22] J. L. Gole and D. A. Dixon, J. Phys. Chem. B **102**, 1768 (1998).
[23] M. D. Mason, G. M. Credo, K. D. Weston, and S. K. Buratto, Phys. Rev. Lett. **80**, 5405 (1998).